

# Magneto-elastic Coupling in the Layered Manganite $\text{La}_{1.2}\text{Sr}_{1.8}\text{Mn}_2\text{O}_7$

C.N. Brosseau<sup>1</sup>, M. Poirier<sup>1</sup>, R. Suryanarayanan<sup>2</sup>, G. Dhahenne<sup>2</sup> and A. Revcolevschi<sup>2</sup>

<sup>1</sup> Centre de Recherche sur les Propriétés Électroniques de Matériaux Avancés and Département de Physique, Université de Sherbrooke, Sherbrooke, Québec, Canada J1K 2R1.

<sup>2</sup> Laboratoire de Physico-Chimie de l'Etat Solide, UMR 8648, Bât. 414, Université Paris-Sud, 91405 Orsay Cédex, France

Received: date / Revised version: date

**Abstract.** We have studied the magneto-elastic coupling in the double layered Mn perovskite  $\text{La}_{1.2}\text{Sr}_{1.8}\text{Mn}_2\text{O}_7$  with an ultrasonic velocity technique. The temperature profile of both the in-plane and out-of-plane longitudinal velocities showed a large stiffening anomaly below the insulating paramagnetic to metallic ferromagnetic transition. Magnetic fluctuations effects consistent with the layered structure are evidenced as a frequency dependent velocity softening above the transition. The magneto-elastic coupling has been studied in magnetic field values up to 8 Tesla: the observations are consistent with a substantial magnetic anisotropy and a ferromagnetic order parameter with moments lying in the layers.

**PACS.** 75.30.Vn Colossal magnetoresistance – 62.65.+k Acoustical properties of solids

## 1 Introduction

Doped perovskite manganites  $\text{La}_{1-x}\text{A}_x\text{MnO}_3$  ( $\text{A} = \text{Sr}, \text{Ca}$ ) are continuing to attract much attention mainly because they are showing a wide variety of magnetic-field induced phenomena like the colossal magnetoresistance (CMR). In these materials, although the double-exchange mechanism [1] serves as a starting point to explain the semiconductor (paramagnetic) to metallic (ferromagnetic) phase transition and the associated CMR, the Jahn-Teller effect and strong electron-phonon interaction must be included into the model [2]. Recent research in these mixed valence manganites has expanded to include the search for materials with other structure types exhibiting CMR. For example, one can adjust the dimensionality of the  $\text{La}_{1-x}\text{Sr}_x\text{MnO}_3$  perovskites by inserting a blocking layer  $(\text{La}_{1-x}\text{Sr}_x)_2\text{O}_2$  between  $\text{MnO}_2$  sheets to yield the Ruddlesden Popper series of compounds with reduced dimension  $n$ ,  $(\text{La}_{1-x}\text{Sr}_x)_{n+1}\text{Mn}_n\text{O}_{3n+1}$  [3, 4, 5, 6]. The compounds  $\text{La}_{1-x}\text{Sr}_x\text{MnO}_3$  belong to this family with  $n = \infty$ . The bilayer perovskite  $(\text{La}_{1-x}\text{Sr}_x)_{n+1}\text{Mn}_2\text{O}_7$  in which two  $\text{MnO}_6$  layers are stacked with  $(\text{La}_{1-x}\text{Sr}_x)_2\text{O}_2$  layers along the  $c$  axis of the structure is obtained for  $n = 2$ . The reduced dimensionality has been shown to have interesting consequences on the physical properties of these compounds. The material is antiferromagnetic (AFM) for  $x = 0$ , while it is ferromagnetic (FM) and exhibits a metal insulator (MI) transition at  $T_c$  in the region  $0.2 \leq x \leq 0.4$ . The maximum  $T_c = 125$  K is obtained for  $x \sim 0.4$  and a large value of CMR is obtained at temperatures near and far

away from  $T_c$  [7, 8]. One of the most distinct features for the bilayered manganites is its anisotropic characteristics in charge transport and in magnetic properties. They offer then a rich opportunity to explore the interplay between spin, charge and lattice degrees of freedom in reduced dimensions. In these materials the magnetization process causes not only a large negative magnetoresistance but also a gigantic anisotropic lattice striction that reveals a complex unconventional spin-charge-orbital coupling [9, 10, 11]. This magneto-elastic coupling is dependent on the magnetic structure and critical phenomena and its role in the mechanism of CMR enhancement has to be clarified.

Neutron diffraction studies [12] have revealed that the low temperature magnetic phase of these compounds consists of planar ferromagnetic (FM) and A-type antiferromagnetic (AFM) components, indicating a canted AFM ordering. For  $x = 0.4$  the canting angle between planes is  $6.3^\circ$  (nearly planar FM). Hirota *et al.* [12] also found that the A-type AFM ordering remained above  $T_c$  and that it showed an anomalous exponential decrease to  $T_N \sim 200$  K. These authors suggested that this AFM phase could play a significant role in the enhancement of CMR effects in this layered Mn system. In another neutron experiment [13], it was shown that the ferromagnetic transition at  $T_c$  which is exhibiting critical scattering and a divergent coherence length is accompanied by 2D ferromagnetic correlations over a wide temperature range. These FM correlations were found to fluctuate rapidly close to  $T_c$ . It was then concluded that the layered manganites provide a unique opportunity to examine in detail the mechanism of the crossover between 2D and 1D magnetism.

In this paper, we investigate with an ultrasonic velocity technique the magneto-elastic coupling in the layered compound  $\text{La}_{1.2}\text{Sr}_{1.8}\text{Mn}_2\text{O}_7$  which is showing the maximum  $T_c$ . Because of a strong coupling between spins and longitudinal acoustic waves, large anomalies are observed on the temperature profile of the acoustic velocity. These anomalies have been studied for different crystal directions in magnetic field values in the range 0-8 Tesla. These data will be discussed in relation with the magnetic structure and with the existence of 2D fluctuations on a wide temperature range. A temperature-magnetic field diagram is proposed.

## 2 Samples and Experiment

Single crystals of  $\text{La}_{1.2}\text{Sr}_{1.8}\text{Mn}_2\text{O}_7$  were grown from the melt by a conventional floating-zone method using a mirror furnace [14]. The compounds crystallize in the body-centered tetragonal structure  $I4/mmm$  ( $D_{4h}^{17}$ ) [15]. The crystals could easily be cleaved to lead to shiny surfaces in the  $ab$  plane with the  $c$  direction perpendicular to it. Neutron diffraction experiments on cm size crystals confirmed the single crystallinity of the sample. For the present experiment, the quality of the single crystal, sliced from a bigger sample, was also checked with optical polarizing microscopy. EDX analysis indicated a homogeneous sample without any extra phases (limit of detection 1%) and further the composition was found to be close to that of the starting material. The ultrasonic velocity is measured with a pulsed acoustic interferometer [16] yielding a sensitivity in relative velocity variation better than 1 ppm. Although the crystals have large dimensions, so large parallel faces that are well suited for pulsed echo ultrasonic measurements, they cannot be used directly. Indeed, the magneto-elastic coupling is so strong and the attenuation (decibel/mm) in the MHz range so high that we had to use much smaller crystals and, doing so, we had to insert a delay line ( $\text{CaF}_2$ ) to separate the ultrasonic echoes. The crystal used in our experiment had dimensions 0.95, 1.15 and 0.75 mm respectively along the  $a$ ,  $b$  and  $c$  axes. One parallel face of the crystal is first glued on the surface of a  $\text{CaF}_2$  delay line (buffer length  $\sim 7$  mm). Then, a  $\text{LiNbO}_3$  piezoelectric transducer bonded on the other parallel face generates longitudinal waves, at 30 MHz and odd overtones, that will propagate through the crystal-delay line ensemble and will be detected by a second piezoelectric transducer at the other end of the buffer. The longitudinal waves can be propagated either along the  $a$  (or  $b$ ) axis or the perpendicular direction  $c$ . Transverse waves have not been used for this study since they could not be isolated easily from other modes in the ultrasonic experiment because of the small dimensions of the crystal.

The temperature profile of the velocity is obtained by monitoring the phase ( $\phi$ ) of the transmitted signal as a function of the temperature. However, since two terms,  $\phi = k_1 l_1 + k_2 l_2$  where  $k_1$ ,  $k_2$ ,  $l_1$  and  $l_2$  are respectively the ultrasonic wave vectors and the lengths of the crystal (1) and the delay line (2), contribute to the total phase of the transmitted signal, it is necessary to subtract the

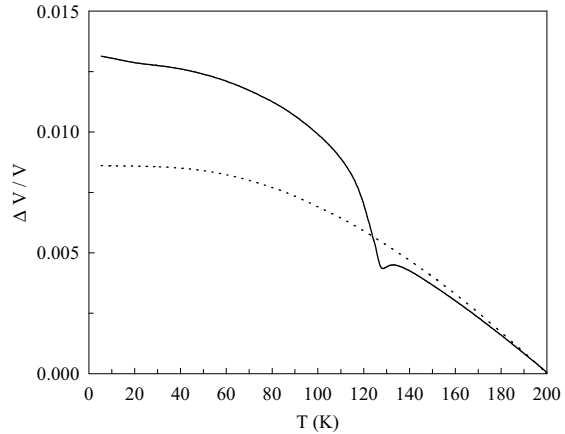


**Fig. 1.** Relative variation of the longitudinal velocity as a function of temperature obtained at 165 MHz: crystal/buffer (full line) and buffer (dotted line).

delay line contribution ( $k_2 l_2$ ) to isolate the crystal one ( $k_1 l_1$ ). The former is measured in a pulsed reflection experiment in the delay line only at the same frequency and for identical experimental conditions. Our ultrasonic data have not been corrected to take into account thermal expansion (striction [9,11]) effects ( $\frac{\Delta l_1}{l_1}$ ) since these are generally orders of magnitude too small compared to the measured relative velocity variation ( $\frac{\Delta v}{v}$ ). The absolute values of the longitudinal velocities are around  $v_{a,b} = 4300$  and  $v_c = 3400$  m/sec. No anisotropy was found between the  $a$  and  $b$  directions. The temperature profile of the velocities is obtained in the range 4-200 K in magnetic field values between 0-8 Tesla. The temperature is monitored either with a Si diode or a carbon glass sensor and stabilized with a LakeShore controller. For reasons of excellent reproducibility during thermal cycling, silicon seal was used for all bonds between the crystal, the transducers and the buffer; no velocity data can be obtained above 200 K where the silicon seal presents a phase transition.

## 3 Results and Discussion

In figure 1 we present an example of the temperature profile of the variation of the velocity (relative to its value at 200 K) for 165 MHz longitudinal waves propagating either through the crystal/buffer ensemble (full line) or the buffer alone (dotted line). The velocity in the buffer shows the usual monotonous behavior which is related to the anharmonic contribution. This means that all the features observed on the crystal/buffer profile are due to magneto-elastic effects in the  $\text{La}_{1.2}\text{Sr}_{1.8}\text{Mn}_2\text{O}_7$  crystal. When the buffer contribution ( $k_2 l_2$ ) to the overall phase ( $\phi$ ) is subtracted, we get the temperature profile of the crystal velocity that is shown in figure 2 for 165 MHz longitudinal waves having their wave vector  $k$  parallel to the  $a$  (or  $b$ ) axis or perpendicular to it ( $k \parallel c$ ). When the temperature is decreased below 200 K for both crystal directions, the

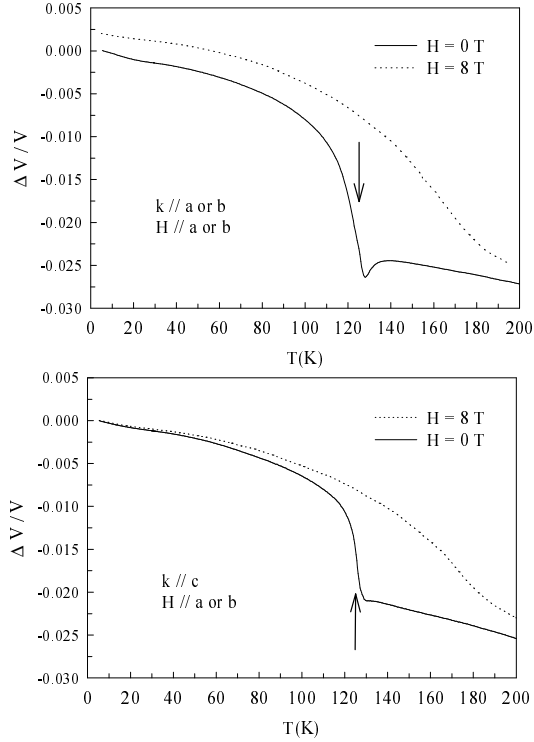


**Fig. 2.** Relative variation of the longitudinal velocity as a function of temperature obtained at 165 MHz:  $k \parallel a$  or  $b$  (upper panel) and  $k \parallel c$  (lower panel). The arrows indicate the transition temperature  $T_c$ .

velocity first increases smoothly but, in the vicinity of the phase transition temperature  $T_c$ , a small softening of the velocity is observed before an important stiffening progressively sets in below  $T_c$ . At low temperatures the smooth behavior is recovered although a small slope increase is seen around 20 K. Differences between the two directions are a larger stiffening anomaly below  $T_c$  and a more pronounced softening around  $T_c$  when waves propagate along the  $a$  (or  $b$ ) axis. As it is observed on the transport properties [8], when a 8 Tesla magnetic field is applied along  $a$  (or  $b$ ), the stiffening anomaly is shifted to higher temperatures as shown in Fig.2. Such a large acoustic anomaly ( $\sim 2\%$  in amplitude) is typical of what is found in strong magnetic materials and we thus suggest to relate it to a magneto-elastic coupling at the paramagnetic-ferromagnetic transition. Indeed, since quasi-particle screening effects are expected to be orders of magnitude smaller and to rather yield a softening anomaly when entering the metallic state below  $T_c$ , the charge degrees of freedom cannot explain the features observed here.

In order to interpret the velocity data presented in Fig.2, we need to define correctly the transition temperature  $T_c$ . This can be done most easily on the temperature profile of the resistivity  $\rho(T)$  where the maximum rate ( $d\rho/dT$ ) generally defines  $T_c$ . We present in figure 3 the microwave resistivity along  $c$  as a function of temperature

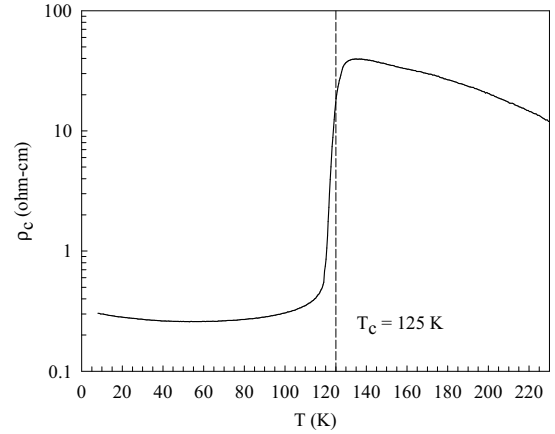


**Fig. 3.** Microwave resistivity (17 GHz) along  $c$  for the layered manganite  $\text{La}_{1.2}\text{Sr}_{1.8}\text{Mn}_2\text{O}_7$  as a function of temperature. The dashed line indicates the transition temperature  $T_c$ .

obtained at 17 GHz on the same crystal. The semiconductor metal transition is characterized by an abrupt decrease of the resistivity at  $T_c = 125$  K where a dashed line indicates the maximum variation of the resistivity. The temperature profile and the transition temperature are similar to the DC ones reported in the literature [8]. In the ultrasonic experiment, this value of  $T_c$  corresponds to the temperature of maximum stiffening rate observed below the weak softening peak as indicated by an arrow in Fig.2.

For  $T < T_c$  the stiffening anomaly is likely due to a coupling between ferromagnetic spins and longitudinal acoustic phonons. Indeed, the stiffening anomalies in zero field shown in Fig.2 are coherent with this picture: a spontaneous magnetization progressively builds up below  $T_c$  and this gives an increase of  $\Delta v/v$ . We have tried to isolate the magneto-elastic coupling by subtracting the anharmonic contribution which is found by extrapolating to low temperatures the profile observed for  $T > T_c$ . The result is presented in figure 4 for both crystal directions. A stiffening anomaly which mimics the magnetization  $M$  of the ferromagnetic phase is obtained. At  $T_c$ , the stiffening appears to be sharper along the  $c$  axis than along  $a$  (or  $b$ ) and the anomalies have different amplitudes, being larger along the  $ab$  plane. A change of slope below 20 K is clearly observed on both curves. Its origin could not be identified as it is hardly modified by a magnetic field and, thus, it will not be discussed further. The softening observed above  $T_c$  is due to magnetic fluctuations and this will be discussed shortly.

The stiffening anomaly can be explained by a magneto-elastic coupling according to the following scenario. We consider a coupling between the strain  $e$  and the order parameter  $Q$  (spin-spin correlation function) and the energy term is phenomenologically expanded in powers of these parameters [17]: a stiffening anomaly below  $T_c$  is obtained if we consider a bi-quadratic coupling energy term  $\lambda e^2 Q^2$ .

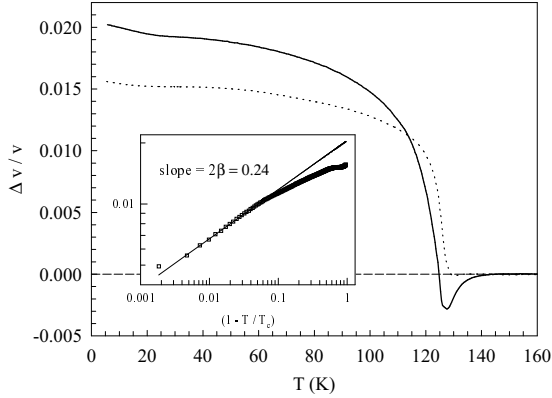


**Fig. 4.** Magneto-elastic contribution to the velocity profile at 165 MHz in zero field: *a* or *b* axis (full line) and *c* axis (dotted line). Inset: *c* axis data as a function of the reduced temperature  $(1 - \frac{T}{T_c})$  on a log-log scale; the straight line represents the best fit in the critical region with  $\beta = 0.12$ .

In most favorable cases where a single ferromagnetic component is present in the low temperature phase and where domain effects are absent, the measurement of the elastic constant  $C$ , so the velocity  $v$  ( $C = \rho v^2$ ,  $\rho$  being the mass density), can reveal the temperature dependence of the order parameter. The curves shown in Fig.4 are in agreement with such a scenario. Since the largest anomaly is observed for in-plane propagation, a larger coupling constant  $\lambda$  is expected. However, ferromagnetic domains are likely present in  $\text{La}_{1.2}\text{Sr}_{1.8}\text{Mn}_2\text{O}_7$  crystals and a AFM component has also been identified in neutron experiments [12] at low temperatures; we thus have to be careful to extract the order parameter from these curves, especially in the critical temperature region. Indeed, the data presented in figure 2 reveal that a 8 Tesla magnetic field oriented along *a* (or *b*) modifies differently the low temperature amplitude of the anomaly according as the wave is propagating parallel or perpendicular to the plane. For the parallel case, a further stiffening likely due to domain wall effects is observed in the ferromagnetic phase when no effects are detected for the perpendicular one.

Longitudinal waves can interact most easily with domain walls that are perpendicular to the elastic polarization. For a tetragonal structure where the Mn magnetic moments are ordered ferromagnetically along the *a* or *b* axes, four domains are expected in zero field and the walls should run preferentially along the *c* axis. The application of a magnetic field will affect the domain structure and the velocity should be changed accordingly. These magnetic field effects investigated at 10 K, far below the critical region, are presented in figure 5 for different configurations of wave propagation and field orientation. In the upper panel we are considering waves propagating along *a* (or *b*). When the field is along the same direction (easy plane), the velocity first softens weakly, reaches a minimum around 0.12 Tesla, then stiffens and saturates above 0.4 Tesla. The minimum could be the result of an increase

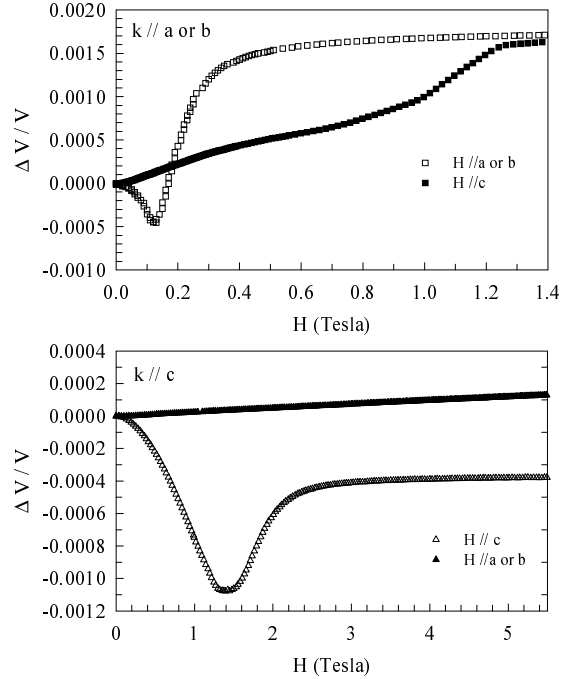


**Fig. 5.** Variation of the velocity relative to its value at zero field at 165 MHz as a function of magnetic field at 10 K. Upper panel, wave vector  $k \parallel a$  or  $b$ ; lower panel,  $k \parallel c$ .

softening due to domain wall motion before stiffening is obtained when the 90 degrees domains rotate to align along the field. When the field is rather along the hard axis (*c*), no minimum is observed and saturation is obtained at a much higher field value around 1.3 Tesla. This is consistent with a large magnetocrystalline anisotropy with the hard axis along the *c* direction; as the domain structure is not modified by a perpendicular field, no softening is observed for this configuration. In the lower panel of Fig.5, we notice that longitudinal waves propagating along *c* are not affected if the field is along *a* (or *b*) since interaction with domain walls is not efficient. For field along *c* however, softening is obtained when the moments are forced to leave the easy plane with a maximum obtained around 1.4 Tesla and saturation is observed above 2 Tesla when all the moments are aligned in the field. The negative value obtained at saturation is likely related to the demagnetization field. This dependence of the velocity in the ferromagnetic phase is fully coherent with the magnetic structure and the field behavior observed by others [18] although the absolute values are somewhat different. In these measurements however, the possible role played by a small AF component is difficult to evaluate.

The effect of domains on the velocity data complicates the determination of the temperature profile of the order parameter, especially the critical behavior near the phase transition temperature. If a bi-quadratic magneto-elastic

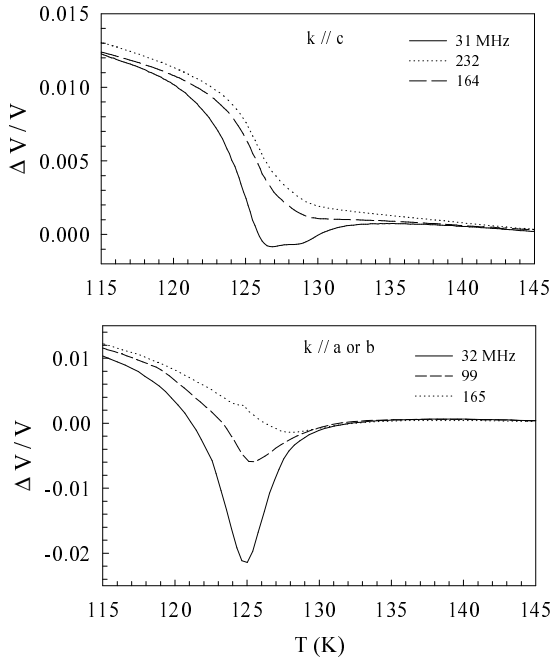


**Fig. 6.** Relative variation of the velocity as a function of temperature near  $T_c$  at different frequencies in the MHz range and in zero field. Upper panel, wave vector  $k \parallel c$ ; lower panel,  $k \parallel a$  or  $b$ .

energy term is used, one can show that the relative velocity change is proportional to the square of the order parameter [17]. Now, if we consider the  $c$  axis velocity data of Fig.4 as being free of magnetic domains effects, the critical region near the phase transition can be fitted reasonably well to the following relation,  $(\frac{\Delta v}{v})^{\frac{1}{2}} \sim Q(T) \sim (T_c - T)^{\beta}$ , with parameters  $T_c = 125.5 \pm 0.2$  K and  $\beta = 0.12 \pm 0.01$  (see inset of Fig.4). The small value of the exponent is consistent with the presence of strongly two dimensional fluctuations below  $T_c$  as predicted by the 2D Ising model ( $\beta = 0.125$ ). If this weak value of  $\beta$  agrees with the neutron scattering data of Osborn et al. [19] and Rosenkranz et al. [20], it contradicts the 3D Heisenberg value (0.35) of Chatterji et al. [21]. However, our results indicate clearly that 2D magnetic fluctuations are dominating the critical temperature region. At much lower temperatures, the  $c$  axis data of Fig.2 (lower panel) reveal that, although a magnetic field shifts the phase transition to higher temperatures, it has no effect on the low temperature value of the order parameter  $Q(0)$ . Such a field independent order parameter  $Q(0)$  has also been observed previously in low-dimensional AFM systems [22,23].

The presence of 2D magnetic fluctuations can also be inferred directly from the velocity data presented in figure 4. Indeed, the velocity softening observed just above  $T_c$  for in-plane propagation can be attributed to fluctuations

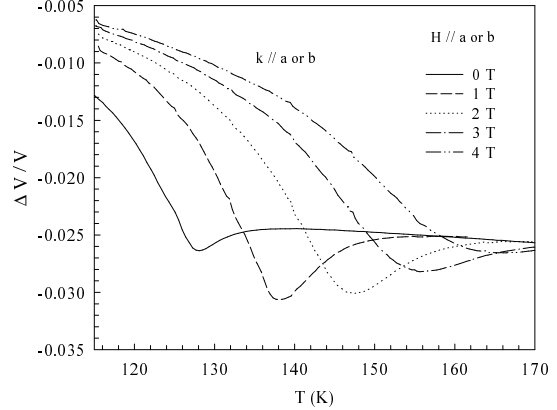


**Fig. 7.** Relative variation of the velocity at 165 MHz as a function of temperature near  $T_c$  for different magnetic field values ( $H \parallel a$  or  $b$ ): wave vector  $k$  oriented along  $a$  or  $b$  axes.

and the fact that this softening is hardly seen for  $c$  axis propagation implies that the fluctuations possess a strong 2D character. In fact, the fluctuation regime for  $T > T_c$  is highly dependent on the frequency in the MHz range. This can be noticed in figure 6 where we present the velocity softening obtained at different ultrasonic frequencies near the transition. For in-plane propagation (lower panel), the amplitude of the softening increases dramatically when the frequency is decreased from 165 to 32 MHz (it reaches more than 2% at the lowest frequency, the same value as the stiffening due to the order parameter below  $T_c$ ) and its maximum comes very close to  $T_c$  (125 K). For out-of-plane propagation (upper panel), a similar effect is obtained but the softening amplitude is much smaller by at least one order of magnitude. This clearly indicates that, for  $T > T_c$ , 2D fluctuations are strongly coupled to acoustic phonons and that their relaxation time is larger than  $10^{-7}$  sec. The range of temperatures over which these fluctuations are extending is difficult to determine since we do not know exactly the temperature profile of the velocity without the effects of spins. According to the data of Fig.6 these fluctuations can be detected at least up to 150 K. This frequency dependence is consistent with the ferromagnetic character of the 2D fluctuations since these are expected to be enhanced as the wave vector  $q \rightarrow 0$ .

It is also well known that the application of a magnetic field can accentuate the fluctuations in low-dimensional magnetic systems. This can be seen in figure 7 where we indicate how the critical region for in-plane propagation is modified by a magnetic field oriented in the plane. In fact, the field is not only shifting the transition temperature to higher values, but it also increases its width. Besides, the amplitude of the softening increases first with field up to 1 Tesla and then decreases smoothly as the critical region becomes wider and wider. The same trend is also observed for out-of-plane propagation with much smaller effects. This behavior is again consistent with the presence of 2D ferromagnetic fluctuations strongly coupled to

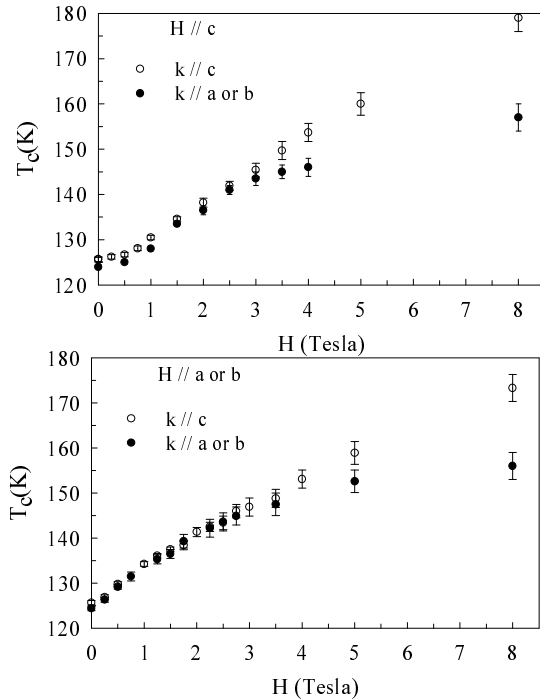


**Fig. 8.** Magnetic phase diagram for both magnetic field orientations:  $T_c(H)$  is determined from the maximum slope of the velocity variation in the critical region for both wave propagation configurations.

acoustic phonons over a wide temperature range above  $T_c$ . Whether the character of the fluctuations is 2D Ising is not fully established since an effective finite-size 2D XY model has been suggested to explain quantitatively the critical properties above and below  $T_c$  [20], although the exponent predicted by this model seems too large (0.23) [24].

Finally, the shift of the transition temperature  $T_c$  as a function of the magnetic field has also been investigated for both wave propagation configurations. The deduced magnetic phase diagram is shown in figure 8. The critical temperature  $T_c(H)$  has been determined with the criterion used in zero magnetic field. As expected, there is essentially no difference between the  $T_c$ 's determined from in-plane and out-of-plane propagation for both orientations of the magnetic field, but only for  $H < 3$ -4 Tesla. For higher field values, the  $T_c$ 's differ surprisingly. We will thus discuss these field ranges separately. When  $0 \leq H \leq 3$  Tesla, the magnetic phase diagram is not dependent on the choice of the wave propagation but it clearly depends on the field orientation. When the field is oriented along one of the easy axes  $a$  or  $b$  (lower panel),  $T_c(H)$  increases quasi-linearly with field up to 1.5 - 2 Tesla with a rate of  $\sim 8$  K/Tesla; for higher fields, the rate gets smaller around 6.3 K/Tesla. For the field oriented along the hard axis  $c$  (upper panel), the relation between  $T_c$  and  $H$  is

rather quadratic at low field values as indicated by the positive curvature noticed in Fig.8. At higher fields ( $H > 1.5$  Tesla), we get a linear increase with a rate similar to the easy plane orientation one. This slower increase of  $T_c$  along the  $c$  axis is coherent with an anisotropy field around 1.5 Tesla as determined previously from the field dependence of the low temperature stiffening anomaly (Fig.5). For  $3 \leq H \leq 8$  Tesla, if  $T_c$  is determined from the  $c$  axis propagation, the linear dependence on field observed below 3 Tesla is maintained up to the maximum value of 8 Tesla.  $T_c(H)$  determined from in-plane wave propagation is however smaller. Since the critical region is much less affected by the fluctuations and domain walls for wave propagation along the hard axis, the true  $T_c(H)$  must be determined from this configuration; in the case of wave propagation along one of the easy axis, fluctuations widen the transition in such a way that  $T_c$  appears to be underestimated. The open circles of figure 8 are thus fully representative of the true phase diagram for this compound.

## 4 Conclusion

We have identified in the layered  $\text{La}_{1.2}\text{Sr}_{1.8}\text{Mn}_2\text{O}_7$  CMR compound an important coupling between longitudinal acoustic phonons and ferromagnetic moments. In the ferromagnetic phase at low temperatures, this coupling produces a stiffening anomaly on the ultrasonic velocity from which the temperature profile of the order parameter, the spin-spin correlation function, could be determined if domain walls effects are taken into account. The field dependence of this stiffening anomaly at low temperatures confirms the known magnetic structure of this compound: an easy plane of magnetization along  $ab$  and a hard axis along  $c$  with an anisotropy field just above 1 Tesla. In the critical region, the exponent of the temperature power law indicates that a 2D Ising model is appropriate to describe the magnetization process. A small anomaly was also observed for  $T < 20$  K but its origin could not be identified. We have also observed above  $T_c$  an important softening of the velocity which confirms that 2D ferromagnetic fluctuations are present in the paramagnetic state over a wide temperature range. However, with our ultrasonic measurements, we could not identify any effects due to the presence of an antiferromagnetic order or fluctuations.

The authors acknowledge the technical assistance of M. Castonguay. This work was supported by grants from the Fonds pour la Formation de Chercheurs et l'Aide à la Recherche of the Government of Québec (FCAR) and from the Natural Science and Engineering Research Council of Canada (NSERC).

## References

1. C. Zener, Phys. Rev. **82**, (1951) 403; P.G. de Gennes *ibid.*, **118**, (1960) 141.
2. A.J. Millis, P.B. Littlewood and B.I. Shraiman, Phys. Rev. Lett. **74**, (1995) 5144; A.J. Millis, B.I. Shraiman and R. Mueller, *ibid.* **77**, (1996) 175.

3. R. Mahesh, R. Mahendiran, A.K. Raychaudhuri and C.N.R. Rao, *J. Solid State Chem.* **122**, (1996) 448.
4. P.D. Battle, S.J. Bludell, M.A. Green, W. Hayes, M. Honold, A.K. Klehe, N.S. Laskey, J.E. Millburn, L. Murphy, M.J. Roseinsky, N.A. Samarin, J. Singleton, N.E. Schluchanko, S.P. Sullivan and J.F. Vente, *J. Phys.: Condens. Matter* **8**, (1996) L427.
5. P. Laffez, G. Van Tendeloo, R. Seshadri, M. Hervieu, C. Martin, A. Maignan and B. Raveau, *J. Appl. Phys.* **80**, (1996) 5850.
6. H. Asano, J. Hayakawa and M. Matsui, *Appl. Phys. Lett.* **70**, (1997) 2303.
7. Y. Morimoto, A. Asamitsu, H. Kuwahara and Y. Tokura, *Nature* **380**, (1996) 141.
8. W. Prellier, R. Suryanarayanan, G. Dhahlenne, J. Berthon, J.-P. Renard, C. Dupas and A. Revcolevschi *et al.*, *Physica B* **259-261**, (1999) 833.
9. T. Kimura, Y. Tomioka, A. Asamitsu and Y. Tokura, *Phys. Rev. Lett.* **81**, (1998) 5920.
10. H. Ogasawara, M. Matsukawa, S. Hatakeyama, M. Yoshizawa, M. Apostu, R. Suryanarayanan, G. Dhahlenne and A. Revcolevschi, *J. Phys. Soc. Japan*, **69**, (2000), 1274.
11. D.N. Argyriou, J.F. Mitchell, C.D. Potter, S.D. Bader, R. Kleb and J.D. Jorgensen, *Phys. Rev.* **B55**, (1997) R11965.
12. K. Hirota, Y. Morimoto, H. Fujioka, M. Kubota, H. Yoshizawa and Y. Endoh, *Jour. Phys. Soc. Japan* **67**, (1998) L3380.
13. D.N. Argyriou, T.M. Kelly, J.F. Mitchell, R.A. Robinson, R. Osborn, S. Rosenkranz, R.I. Sheldon and J.D. Jorgensen, *J. Appl. Physics* **83**, (1998) 6374.
14. A. Revcolevschi and R. Collongues, *C.R. Acad. Sci.*, **266**, (1969) 1767.
15. J.F. Mitchell, D.N. Argyriou, J.D. Jorgensen, D.G. Hinks, C.D. Potter and S.D. Bader, *Phys. Rev.* **B55**, (1997) 63.
16. M. Poirier, A. Caillé and M.L. Plumer, *Phys. Rev.*, **B41**, (1990) R4869.
17. J.P. Pouget, in *Low-Dimensional Electronic Properties of Molybdenum Bronzes and Oxides*, edited by C. Schlenker (Kluwer Academic, Netherlands, 1989), pp. 87-157.
18. R.P. Sharma, P. Fournier, R.L. Greene, T. Venkatesan, J.F. Mitchell and D. Miller, *Jour. Appl. Phys.* **83**, (1998) 7351.
19. R. Osborn, S. Rosenkranz, D.N. Argyriou, L. Vasiliu-Doloc, J.W. Lynn, S.K. Sinha, J.F. Mitchell, K.E. Gray and S.D. Bader, *Phys. Rev. Lett.* **81**, (1998) 3964.
20. S. Rosenkranz, R. Osborn, L. Vasiliu-Doloc, J.W. Lynn, S.K. Sinha and J.F. Mitchell, *cond-mat/9909059*.
21. T. Chatterji, P. Thalmeier, G.J. McIntyre, R. van de Kamp, R. Suryanarayanan, G. Dhahlenne and A. Revcolevschi, *Europhys. Lett.* **46**, (1999) 801.
22. S. Allen, J.-C. Piéri, C. Bourbonnais, M. Poirier, M. Matos and R.T. Henriques, *Europhys. Lett.* **32**, (1995) 663.
23. M. Poirier, M. Castonguay, A. Revcolevschi and G. Dhahlenne, *Phys. Rev.* **B52**, (1995) 16058.
24. S.T. Bramwell and P.C.W. Holdsworth, *J. Phys: Condens. Matter* **5**, (1993) L53; *Phys. Rev. B* **49**, (1994) 8811; S.T. Bramwell, P.C.W. Holdsworth and M.T. Hutchings, *J. Phys. Soc. Jap.* **64**, (1995) 3066.